MIXED CONVECTION IN FERROFLUIDS VERTICAL LAYER WITH INCLINED MAGNETIC FIELD

Md. Habibur Rahman[*], Mst. Lovly Khatun and Sushmita Mondal

Department of Mathematics, Khulna University of Engineering & Technology, Khulna-9203, Bangladesh

ABSTRACT

In this article, the flow characteristics and linear stability of mixed convection in a ferrofluid layer are investigated. The fluid layer is positioned between two vertically oriented and differently heated nonmagnetic plates under an inclined magnetic field with non-zero gravity. This study involves the patterns of fluid motion, heat transfer, and the effects of the inclined magnetic field with gravitational action. The objective of this article is to analyze the flow characteristics of smaller Prandtl number of fluid and figure out the significant comparisons with larger Prandtl numbers of fluids. The characteristic of every instability mode is examined for a fluid having a different Prandtl number than that one which was previously investigated. The influence of buoyancy effects undergoes a notable transformation, shifting from a destabilizing role in flows dominated by gravity to a stabilizing role in flows characterized by stronger magnetic effects. It is found that in both normal and oblique magnetic fields, the basic flow evolves into a state of greater stability, and wave propagation is faster with lower Prandtl numbers of fluids than with larger Prandtl numbers of fluids.

Keywords: Convection, Ferrofluids, Instability, Magnetic field.

1. INTRODUCTION

Ferromagnetism is a solid-state phenomenon that emerges at an elevated energy state that is less favorable for the material. When solid magnetic nanoparticles (such as cobalt, iron, nickel, and their alloys) with a characteristic diameter of approximately $d_p \sim 10$ nm are immersed in a molten state and coated with a surfactant layer. According to Odenbach (2002), a typical ferromagnetic fluid can be blended with magnetic materials up to 10% and surfactant up to 10% by volume. Artificial magnetic fluids, commonly referred to as ferrofluids, are specialized liquids that exhibit strong magnetization in response to magnetic fields. The term 'ferrofluid' is derived from a combination of 'fluid' and 'ferromagnet', emphasizing their unique properties. This phenomenon arises due to the presence of microscopic magnetic particles within the fluid, which can be about 100 times smaller in size compared to the visible light wavelength. These particles play a crucial role in enabling the strong magnetization of ferrofluids. Non-conducting artificial ferrofluids are often composed of colloids of iron oxides such as magnetite (Fe_3O_4) and hematite (Fe_2O_3), which consist of tiny ferromagnetic particles dispersed in a liquid carrier, usually synthetic oil or kerosene. To stop the formation of iron oxide aggregates and the subsequent sedimentation of these aggregates, oleic acid is used as a common surfactant molecule.

Ferrofluids have been discovered to have numerous practical applications in electronic devices, vitality transformation gadgets, oil separation from water, tunable optical channels, scientific instrumentation, deformity identification sensors, mechanical, pharmaceutical, aeronautic, and so on. Ferrofluid can be used in the field of magnetic resonance imaging as a contrast agent and to detect cancer. Ferrofluids have a wide application in industry. As indicated by Finlayson (1970), the industrial-scale production of these fluids became prominent during the 1960s and 1970s. Nowadays, their manufacturing technique has substantially improved, allowing a variety of ferrofluid applications for development. Ferrofluids do not maintain magnetization in the absence of an outside magnetic field and are thus frequently classified as super-paramagnets rather than ferromagnet, as explained by Albrecht et al. (1997). The Curie effect describes how the magnetization of a solid magnetic phase varies with temperature. The temperature at which an element loses its natural magnetic properties is denoted by the Curie temperature, also referred to as the Curie point.

The atom vibrations start to disrupt this proper alignment when the temperature rises over a certain point; at temperatures greater than the Curie temperature, this alignment is totally destroyed. Above the Curie temperature, the magnetic material transforms into a paramagnetic substance. It has been discovered that a ferromagnetic material is nonmagnetic when the Curie temperature remains lower than its melting temperature.

Magnetic fluids, in contrast, are multi-phase liquids containing substantial particles of magnetic material that can be magnetized.

The manipulation of heat and mass transfer within these liquids can be attained by applying an externally generated magnetic field, and such suspensions can be employed to transmit heat. The main procedures of the analyses described in (Finlayson, 1970; Suslov, 2008; Belyaev & Smorodin, 2010; Suslov, 2012) and particularly Rahman and Suslov (2016) will be followed in this article, with a focus on the assessment of thermal effects and the impacts of the position, including the strength of the magnetic field, on the behaviors of fluid. This paper investigates a variety of motivating variables derived from the experimental observations mentioned in (Suslov, 2012; Bozhko & Putin, 1991, 2003; Bozhko-*et al.* 1998). The observed ferrofluid motions associated with controlling the physical mechanisms will be clarified theoretically. In order to better understand the resulting aspects due to the conflict between convective thermograviational and thermomagnetic mechanisms, fluids with strong and weak degrees of magnetization will be developed, respectively, for the comparative findings in a different Prandtl number of fluid than previous investigations (Finlayson, 1970; Suslov, 2008; Rahman & Suslov, 2015, 2016) and references within them. The mixed convective flow of kerosene-cobalt ferrofluid in a lid-driven square cavity under partial slip conditions is numerically investigated by Chamkha et al. (2020) using the finite volume approach. To maintain the horizontal moving walls adiabatic, they created an enclosure with two vertical walls that were partially heated at a constant temperature. The rate of heat transfer under the influence of the magnetic field and the movement of opposite-directional horizontal walls is discovered to be affected by the increase in the volume percentage of ferromagnetic particles. Due to the dissipation of the boundary layer gradient, the magnetic field's influence slows the rate of heat transmission. In contrast, as the horizontal walls moved in the opposing directions, the rate of heat transmission increased. Taskesen et al. (2023) studied the experimental findings using mono (Fe_3O_4 and Cu) and hybrid (Fe_3O_4 -Cu) type water-based nanofluids with extremely low nanoparticle volume concentrations in laminar flow conditions and contrasted them with findings from an artificial neural network (ANN). These findings demonstrate that a suitable feasible way by using ANN to forecast how well hybrid nanofluid will perform in terms of convective heat transfer rate under the influence of a magnetic field.

To understand the physics of a complex flow behavior of magnetic fluids, and also to obtain a vital information for industrial applications, a systematic study through a proper theory is important. Therefore, the goal of this study is to investigate various convective instabilities in ferromagnetic fluids influenced by buoyancy and ponderomotive force due to magnetic effects. Fluids used in most of the technologically important applications are non-isothermal. That is why the study of convection and heat transfer is needed. Since ferrofluids respond to both thermal and magnetic fields, their physical and mathematical description is a challenging task. Typically, a set of constitutive equations: continuity equation, Navier-Stokes equation, thermal energy equation, along with the Maxwell equations is used involving a constant viscosity assumption.

The convective flow instability patterns in larger Prandtl numbers of ferromagnetic fluids when the applied field is normal to the plates are investigated by Suslov (2008). However, Rahman and Suslov (2015, 2016) analyzed various convective instabilities in larger Prandtl numbers of ferromagnetic fluids under the inclined magnetic field effects on the layer. The novelty of this article is to investigate various convective instabilities in smaller Prandtl numbers of ferromagnetic fluids in both cases of normal and inclined magnetic field effects, as well as provide significant comparisons with larger Prandtl numbers of fluids.

2. THEORETICAL BACKGROUND

As depicted in Fig. 1, we consider a ferromagnetic fluid layer positioned within two vertical, magnetically inactive plates that are infinitely stretched. The right-handed rectangular coordinate form (x, y, z) is centered at the origin, while the plates are positioned at $x = \pm d$. In addition, the gravity vector $\vec{g}$ is characterized by the components (0, -g, 0). A consistent temperature of $T_* \pm \theta$ is maintained for the plates. The plates are subjected to an external and consistent magnetic field with an intensity of H^e and some inclinations. Assume that δ is an angle of inclination magnetic field associated with the x-axis so that $H_x^e = H_e \cos \delta$, $H_y^e = H_e \sin \delta \cos \gamma$ and $H_z^e = H_e \sin \delta \sin \gamma$ are its components in the directions of the rectangular coordinate axes of x, y and z respectively, where γ represents the angle formed by its projection line relative to the vertical axis. In another sense, the application of a magnetic field induces a magnetic field $\vec{H}$ within the fluid, with a magnitude denoted as H. The magnetic field causes the fluid to become magnetized, $\vec{M}$ to the point where $|\vec{M}| = M$, which is thought to be co-directed in accordance with the fluid's interior magnetic field, such as $\vec{M} = \chi_* \vec{H}$, where χ_* indicates the fluid's integral magnetic susceptibility. Due to ferrofluids' low electrical conductivity, the Boussinesq approach with regard to the basic equations of continuity (2.1), Navier-Stokes (2.2), as well as heat energy (2.3), are also taken into consideration, along with the Maxwell equations (2.4), regarding the magneto-static manner of magnetic field (Rosensweig, 1985). For the problem, the dimensionless governing equations

involving velocity $\vec{v} = (u, v, w)$, magnetic field $\vec{H}$, pressure p, temperature T, and fluid magnetization $\vec{M}$ can be expressed as follows:
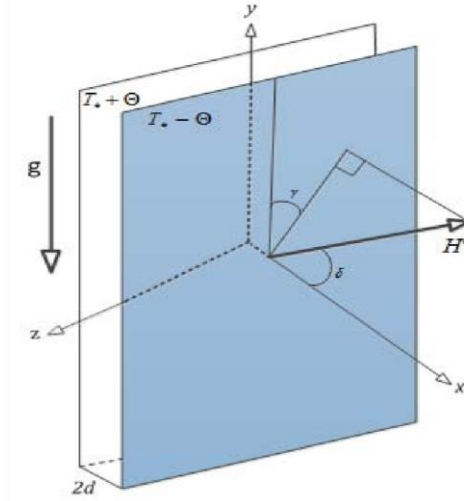

Figure 1: The schematic view for the problem geometry.

$$\nabla . \vec{v} = 0, \tag{2.1}$$

$$\rho_* \frac{\partial \vec{v}}{\partial T} + \rho_* \vec{v} . \nabla \vec{v} + \nabla p = \eta_* \nabla^2 \vec{v} + \rho \vec{g} + \mu_0 M \nabla H, \tag{2.2}$$

$$\frac{\partial T}{\partial t} + \vec{v} . \nabla T - \kappa_* \nabla^2 T = 0, \tag{2.3}$$

$$\nabla \times \vec{H} = \vec{0}, \ \nabla . \vec{B} = 0, \tag{2.4}$$

$$\vec{B} = \mu_0 (\vec{H} + \vec{M}) \ \text{and} \ \vec{M} = \frac{M (H,T)}{H} \vec{H}, \tag{2.5}$$

where ρ_* denotes density, t time, p pressure, T temperature, η_* dynamic viscosity, κ_* thermal diffusivity, $\vec{B}$ magnetic flux density, and μ_0 magnetic constant. The fluid properties estimated at the center point of the problem geometry are denoted by the subscript $*$, and that point T_* is identified as reference temperature. The Boussinesq approximation is applicable under the assumption of a small temperature, and the variation in fluid density is assumed to be:

$$\rho = \rho_* [1 + (T_* - T)\beta_*], \tag{2.6}$$

where $\beta*$ defines the thermal expansion coefficient at $T*$. The governing equations, along with the corresponding boundary conditions, are nondimensionalized using length, temperature, thermodynamic pressure, and velocity as the reference quantities

$$(x, y, z) = d(x', y', z'), \text{t} = \frac{\rho_* d^2}{\eta_*} t', P = \frac{\eta_*^2}{\rho_* d^2} P', \vec{v} = \frac{\eta_*}{\rho_* d} \vec{v}', \&$$

$$\vec{g} = g\vec{e}_g, \Delta\text{T} = \Theta\theta', \vec{H} = \frac{\kappa\Theta}{1 + \chi} \vec{H}', \vec{M} = \frac{\kappa\Theta}{1 + \chi} \vec{M}',$$

where, d is half of the distance between two vertical walls and the gravity $\vec{e}_g = (0, -1, 0)$. Afterward, for the sake of simplicity in notation, we eliminate all the primes, resulting in the following equations:

$$\nabla . \vec{v} = 0, \tag{2.7}$$

$$\frac{\partial \vec{v}}{\partial t} + \vec{v} . \nabla \vec{v} + \nabla P = \nabla^2 \vec{v} - Gr\theta \vec{e}_g - Gr_m \theta \nabla H, \tag{2.8}$$

$$\frac{\partial \theta}{\partial t} + \vec{v} . \nabla \theta - \frac{1}{Pr} \nabla^2 \theta = 0, \tag{2.9}$$

$$\nabla \times \vec{H} = \vec{0}, \tag{2.10}$$

$$\nabla . \vec{H}(1 + \chi_*) + \nabla H . \vec{e_*} (\chi - \chi_*) - \nabla \theta . \vec{e_*} (1 + \chi) = 0, \tag{2.11}$$

$$\vec{M} = \vec{e_*} [(H - N)(\chi - \chi_*) - \theta(1 + \chi)] + \chi_* \vec{H}, \tag{2.12}$$

with the following boundary conditions:

$$[\vec{H}^e - \{(H - N)(\chi - \chi_*) \mp \vec{e}^*(1 + \chi)\} - \vec{H}(1 + \chi_*)].\vec{\eta} = 0, \tag{2.13}$$

$$\vec{v} = \vec{0} \ and \ \theta = \mp 1 \ at \ x = \pm 1. \tag{2.14}$$

These are the parameters with no dimensions that exist in the problem as follows:

$$Gr = \frac{\rho_*^2 \beta_* \Theta g d^3}{\eta_*^2}, Gr_m = \frac{\rho_* \mu_0 K^2 \Theta^2 d^2}{\eta_*^2(1 + \chi)}, Pr = \frac{\eta_*}{\rho_* K_*}, N = \frac{H_*(1 + \chi)}{K\Theta}. \tag{2.15}$$

where, H_* denotes the magnitude of magnetic field $\vec{H}_*$, is calculated at T_*. The Grashof numbers regarding magnetic and thermal forces, denoted as Gr_m and Gr respectively, quantify the significance of magnetic and buoyancy forces. The Prandtl number, denoted as Pr, signifies the proportion of the momentum diffusivity related to the thermal conductivity, which can be used to calculate heat transfer and free and forced convection depending on fluid properties. When fluid magnetization varies due to temperature variables, parameter N, which measures the magnetic field strength at the point of reference. Here, Grashof numbers are assigned to certain values in order to build the whole parametric instability region. Flow stabilization is influenced by the kind of fluid, which is represented by viscosity and, as a result, the fluid's Prandtl number. We choose the Prandtl number Pr as 27.5 and let $\chi = \chi_* = 3$ (for linear magnetization) as well as the unequal values such as $\chi = 3, \chi_* = 5$ (for nonlinear magnetization regime) as in the experiment of (Bozhko-*et al.* 2013). In agreement with (Rahman & Suslov, 2015), we have also chosen lower values of $\chi = 0.5$ and 1.5, as well as $\chi = 1.5$ and 2.5, which are magnetic states that are close to saturation.
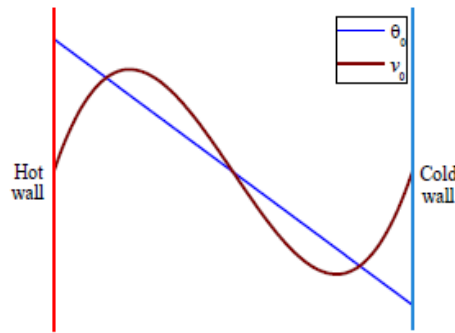

Figure 2: Basic convective flow pattern.

Equations (2.7)--(2.14) have steady-state solutions in the form

$$\vec{v}_0 = (0, v_0(x), 0), P_0 = P_0(x), \theta_0 = \theta_0(x), \vec{H}_0 = (H_{x0}(x), H_{y0}, H_{z0}).$$

They should satisfy

$$D^2 v_0 = -Gr\theta_0, DP_0 = -Gr_m \theta_0 e_{10} DH_{x0}, D^2 \theta_0 = 0, \tag{3.1}$$

$$DH_{x0}(1 + \chi_*) + e_{10} e_{10*} DH_{x0}(\chi - \chi_*) - e_{10*} D\theta_0(1 + \chi) = 0, \tag{3.2}$$

$$DH_{y0} = 0, DH_{z0} = 0, \tag{3.3}$$

Using the following boundary conditions

$$H_x^e - e_{10*}(H_0 - N)(\chi - \chi_*) - H_{x0}(1 + \chi_*) \pm e_{10*}(1 + \chi_*) = 0, \tag{3.4}$$

$$H_{y0}(x) = H_y^e, H_{z0}(x) = H_z^e, \theta_0 = \pm 1 \ at \ x = \mp 1. \tag{3.5}$$

The basic and thermal velocity profiles in the flow domain are depicted in the Fig. 2. The linearization of equations (2.7) – (2.14) regarding the basic form and using the generalized Squire's transformations

$$(x, y, z) = (\tilde{x}, \tilde{y}, \tilde{z}), \theta_0 = \tilde{\theta}_0, H_{x0} = \tilde{H}_{x0}, H_0 = \tilde{H}_0, \alpha^2 + \beta^2 = \tilde{\alpha}^2, \beta = \tilde{\beta},$$
$$\sigma = \tilde{\sigma}, u_1 = \tilde{u}, \alpha v_1 + \beta w_1 = \tilde{\alpha} \tilde{v}, w_1 = \tilde{w}, P_1 = \tilde{P}, \theta_1 = \tilde{\theta}, \phi_1 = \tilde{\phi},$$
$$\alpha Gr = \tilde{\alpha} \tilde{G}r, Gr_m = \tilde{G}r_m, Pr = \tilde{P}r, \chi_* = \tilde{\chi}_*, \chi = \tilde{\chi}, e_{10*} = \tilde{e}_{10*},$$
$$e_{10} = \tilde{e}_{10}, \alpha e_{20} + \beta e_{30} = \tilde{\alpha} \tilde{\beta} b, \alpha e_{20*} + \beta e_{30*} = \tilde{\alpha} \tilde{e}_{20*}. \tag{3.6}$$

By noting $\alpha v_0 = \tilde{\alpha} \tilde{v}_0, \tilde{v}_0 = \tilde{G}r(\tilde{x}^3 - \tilde{x})/6$, and finally, removing all the tilde notations for avoiding complexity in the write-up without loss of generality lead to the following equations:

$$Du + i\alpha v = 0, \tag{3.7}$$

$$\sigma u + (\alpha^2 + i\alpha v_0 - D^2)u + DP + e_{10} Gr_m DH_{x0}\theta + Gr_m \theta_0 e_{10} D^2 \phi \tag{3.8}$$

$$+Gr_m \theta_0 \left[i\alpha e_{20} + (1 - e_{10}^2)\frac{DH_{x0}}{H_0}\right]D\phi - i\alpha Gr_m \theta_0 e_{10} e_{20} \frac{DH_{x0}}{H_0}\phi = 0,$$

$$\sigma v + Dv_0 u + (\alpha^2 + i\alpha v_0 - D^2)v + i\alpha P - Gr \theta + \alpha Gr_m \theta_0 (ie_{10} D\phi - \alpha e_{20}\phi) = 0, \tag{3.9}$$

$$\sigma w + (\alpha^2 + i\alpha v_0 - D^2)w + i\beta P + \beta Gr_m \theta_0 (ie_{10} D\phi - \alpha e_{20}\phi) = 0, \tag{3.10}$$

$$\sigma\,\theta + D\,\theta_0 u + \left(\frac{\alpha^2 - D^2}{Pr} + i\alpha v_0\right)\theta = 0, \tag{3.11}$$

$$(D^2 - \alpha^2)\,\phi - \frac{\chi - \chi_*}{1 + \chi_*}\,\alpha e_{20}\left[\alpha e_{20*} + ie_{10*}\,e_{10}\,\frac{DH_{x0}}{H_0}\right]\phi \tag{3.12}$$

$$+\frac{\chi - \chi_*}{1 + \chi_*}\left[i\alpha\,(e_{10}\,e_{20*} + e_{10*}\,e_{20}) + e_{10*}\,(1 - e_{10}^2)\,\frac{DH_{x0}}{H_0}\right]D\phi$$

$$+\frac{\chi - \chi_*}{1 + \chi_*}e_{10*}\,e_{10}D^2\phi - \frac{1 + \chi}{1 + \chi_*}\,[i\alpha e_{20*} + e_{10*}D]\theta = 0,$$

and the boundary conditions

$$(1 + \chi_*)D\phi \pm |\alpha|\,\phi + e_{10*}\,(\chi - \chi_*)\,(i\alpha e_{20} + e_{10}D)\,\phi = 0, \tag{3.13}$$

$$u = v = w = 0 \text{ and } \theta = 0 \text{ at } x = \pm 1. \tag{3.14}$$

Furthermore, the aforementioned linearized equations are solved numerically. The obtained results are then comprehensively analyzed and appropriately plotted in accordance with the requirements of the subsequent section 5.

3. METHODOLOGY

The resulting linearized equations (3.7) – (3.12) using boundary conditions (3.13) and (3.14) are discretized, and the numerical results are obtained by utilizing the pseudo-spectral Chebyshev expansion methods, which are reported in (Ku & Hatziavramidis, 1984) and (Hatziavramidis & Ku, 1985) and implemented in Suslov and Paolucci (1995) and Rahman and Suslov (2015, 2016). This spatial approximation converges exponentially quickly, and thus 61 colocation points are utilized in the present computations for significant numerical results. The numerical results of this problem are obtained by solving the corresponding equations with the help of MATLAB software. The eigenvalue problems are solved by using the MATLAB function eig.

4. RESULTS AND DISCUSSION

4.1 Characteristics in Normal Magnetic Field

The present study encompasses a thorough investigation of the stability characteristics of convection flow. This analysis considers a wide range of Prandtl numbers, arbitrarily chosen field inclination angles, as well as both linear and nonlinear magnetization behaviors of liquids. There are three primary forms of instability structures in a normal magnetic field: magnetic, magneto-gravitational, and thermogravitational convections. The corresponding eigenvalue patterns are illustrated in Figs. 3, 4, and 5. It is clear from Fig. 3 that, in the state of thermogravitational instability ($Gr_m \rightarrow 0$), the highest value of the disturbance the amplifying rate σ^R exists, accompanied by eigenvalues that are complex conjugate indicating the presence of two reverse-propagating waves. According to Fig. 4, there is another highest value of the disruption amplification rate σ^R, however in this event ($Gr \rightarrow 0$), the eigenvalues are realistic, and this circumstance relates to a static magneto-convection pattern. In the third scenario, when $Gr_m \neq 0$ and $Gr \neq 0$, it is possible for up to three maximum values of the disruption amplification rate σ^R to occur (refer to Fig. 5). The leftmost and rightmost maxima correspond to waves with smaller and larger wave numbers, respectively, while the middle maximum represents a stationary magneto- convection trend.

The stability modes that begin with ($Gr_m = 0$, $Gr \neq 0$), ($Gr_m \neq 0$, $Gr = 0$), and ($Gr_m \neq 0$, $Gr \neq 0$) are usually referred as thermogravitational, magnetic, and magneto-gravitational convections, respectively. Rahman and Suslov investigated the crucial values for the Grashof number, Gr_m, namely 0, 12, and 30, as stated in (Rahman and Suslov, 2016). Their observations revealed that when Gr_m is low. Conversely, for higher values of Gr_m, the value of α initially increases, but then decreases with increasing Prandtl number Pr. In this study, we used 35 as high values and 5 and 10 for Gr_m as low values, and the same characteristic is observed as stated in (Rahman and Suslov, 2016) [see Table 1]. In other words, when Gr_m is low, α_c grows, but when Gr_m is large, α_c first increases and then reduces as Pr increases. As the data in Table 1 demonstrate, without the presence of buoyancy force (i.e., $Gr = 0$), when Pr increases, the critical value of Gr_m reduces while α_c continues as a constant. In other words, the wave number is unaffected by the values of Pr at the beginning of a magneto-static convection (when $Gr = 0$).
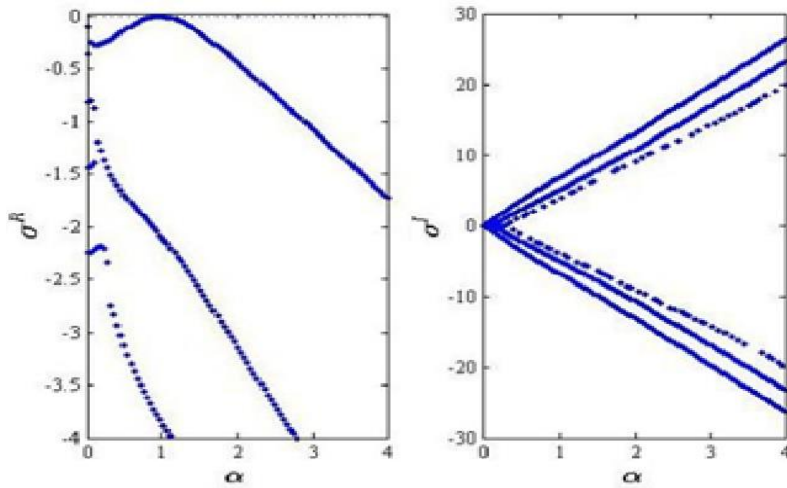
Figure 3: The leading spreading spatial amplifier distribution rates σ^R (in the left plot) and the frequency σ^I (in the right plot) as the functions of α for $(Gr_m, Gr) = (0, 107.825)$ (threshold of thermogravitational convection) at $Pr = 27.5$, $\chi = \chi_* = 5$, $\gamma = 0°$ and $\delta = 0°$.
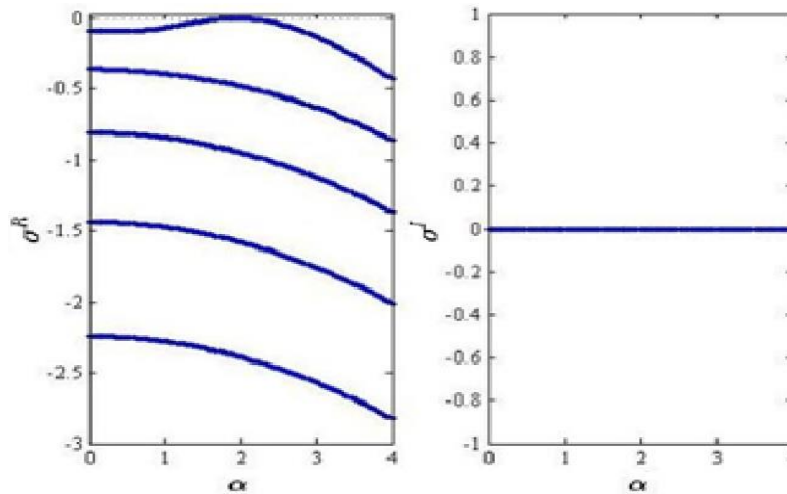

Figure 4: The similar values as Fig. 3 except for $(Gr_m, Gr) = (6.609, 0)$ (threshold of stationary magneto-convection).
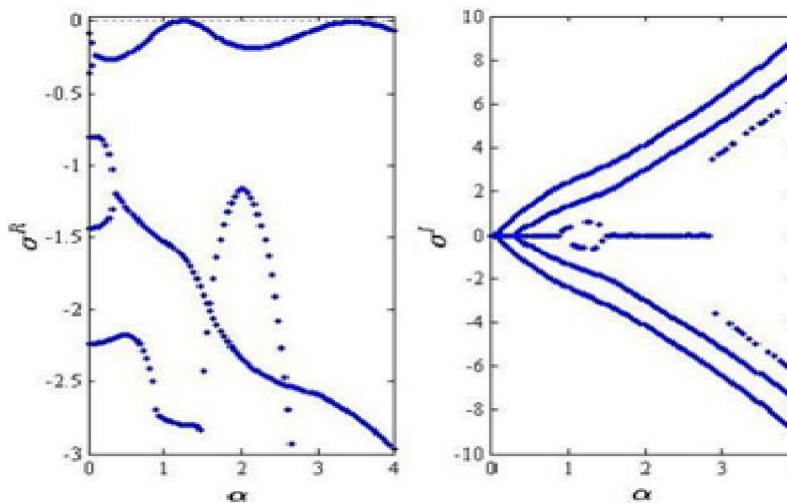

Figure 5: The similar values as Fig. 3 except for $(Gr_m, Gr) = (124, 41.61)$. The middle optimum in the left figure related to a stationary roll structure, while the maxima exist in the both ends are related to minor and

greater wave numbers, respectively.

Table 1: The crucial parameters values of Gr_m-magnetic Grashof number, Gr-thermal Grashof number, α-wave number, c-propagating wave speed and $v_{0\max}$-the maximum basic flow speed for the mixed convection in the normal ($\delta = 0°$) magnetic field with strength $H^e = 100$ for $\chi = \chi_* = 5$ with different values of Pr.

Pr	Gr_{mc}	Gr_c	α_c	c_c	$v_{0\max}$
20	5	149.980	0.824	±9.232	9.616
27.5	5	106.487	0.969	±6.662	6.828
55	5	62.979	1.153	±4.040	4.038
70	5	54.044	1.200	±3.489	3.465
130	5	37.108	1.308	±2.423	2.379
150	5	33.967	1.333	±2.222	2.178
20	10	149.083	0.828	±9.172	9.559
27.5	10	105.109	0.978	±6.568	6.739
55	10	60.389	1.183	±3.862	3.872
70	10	50.931	1.241	±3.274	3.266
130	10	31.987	1.401	±2.070	2.051
150	10	28.063	1.447	±1.815	1.799
20	35	144.378	0.845	±8.855	9.257
27.5	35	97.399	1.025	±6.043	6.245
55	35	38.291	1.459	±2.354	2.455
60	35	23.748	1.651	±1.395	1.523
65	35	11.036	1.498	±0.535	0.708
70	35	8.733	1.350	±0.382	0.560
75	35	7.710	1.234	±0.269	0.453
20	9.087	0.0	1.936	0.0	0.0
27.5	6.609	0.0	1.936	0.0	0.0
55	3.305	0.0	1.936	0.0	0.0
70	2.596	0.0	1.936	0.0	0.0
130	1.398	0.0	1.936	0.0	0.0
150	1.212	0.0	1.936	0.0	0.0

The data in Table 1 further indicates that the stationary magneto-convection pattern is defined by Gr_m, which is inversely proportional to Pr. One can conclude that in a fluid with a large Prandtl number, the disruption wave speed associated with gravitational instability patterns surpasses the optimal velocity of the basic flow. This suggests that the physical properties of instabilities are independent of the velocity field of the base flow. The basic flow actually gets less stable as the Prandtl number increases due to its definition as the ratio of fluid viscosity to thermal diffusivity; a high Prandtl number signifies reduced thermal diffusion. As a result, thermal spreading waves dissipate slowly in fluids with a high Prandtl value. Based on the data in Table 1, it is possible to figure out that the fundamental physical structure of the instabilities seen for $Gr_m = 0$ is thermally dominant. Thermal waves move upwards close to the hot wall as well as downwards towards the cold wall (refer to Table 2 for further information).

When both Gr and Gr_m are something other than zero, this conclusion is mostly accurate for magneto-gravitational convection. Table 2 shows the typical critical values of Gr, α, and c in a normal magnetic field regarding two thermomagnetic waves at Pr = 27.5 and $Gr_m = 12$ with different values of χ and χ_*. Within the framework of the linear magnetization law, the two waves propagate in opposite directions while maintaining equal velocities. The propagating waves possess an identical wave number, resulting in the instability of the basic flow in response to the simultaneous propagation of both upward and downward waves. An example of such a case is the nonlinear magnetization law, where the presence of different values for χ and χ_* disrupts the wave's symmetry. As a result, the first wave, which is the upward wave adjacent to the hot wall, becomes more critical compared to the second wave, which is the downward wave near the cold wall (refer to Table 2). The upward wave is identified by a slightly higher wave number than the downward wave.

Table 2: The crucial parameters values of Gr, α as well as c for two prominent waves of the mixed convection in the normal ($\delta = 0^{\circ}$) magnetic field with strength $H^e = 100$ for $Gr_m = 12$, $Pr = 27.5$, $\gamma = 0^{\circ}$ with different values for χ and χ_*.

		Upward propagating wave			Downward propagating wave		
χ	χ_*	α_c	Gr_c	c_c	α_c	Gr_c	c_c
5	5	0.981	104.54	6.630	0.981	104.54	-6.530
3	5	0.979	105.43	6.582	0.976	106.07	-6.623
3	5	0.982	104.25	6.510	0.982	104.25	-6.510
1.5	2.5	0.984	104.19	6.502	0.981	104.73	-6.538
1	2	0.982	104.47	6.519	0.978	105.36	-6.577
0.5	1.5	0.977	105.77	6.599	0.968	107.64	-6.720

4.2 Instability Characteristics in Inclined Magnetic Field

The critical parameter values; Gr, α as well as c of mixed convection for the first and second waves for $Pr = 27.5$, $Gr_m = 12$, $\gamma = 0^{\circ}$ are shown in the Table 3 and Table 4, respectively (see odd number lines for $H^e = 100$) and (see even number lines for $H^e = 10$) for different values of χ as well as χ_*. In these tables, the critical values of various values of δ for χ as well as χ_* are shown. According to the data of Table 3 and Table 4, the basic flow gets more stable when the field angle rises. With an increase in the field inclination angles, there is a reduction in the wave numbers, resulting in a greater distance between the two instability rolls. Simultaneously, the spreading waves exhibit faster propagation with higher field inclination angles.

The inclined magnetic field causes wave propagation to be asymmetric compared to normal fields, regardless of the magnetization of the fluid in the flow domain shown in Tables 3 and 4. There is a definite pattern of upward wave propagating in different inclination magnetic fields, which is always identified by a larger number of wave than the downward one. In linear magnetization laws, the basic flow of upward wave propagation is less stable than downward wave propagation. Consequently, the upward propagation waves stay in the most hazardous in inclining magnetic fields. Compared to the wave moving in the other direction, the upward wave moves more slowly than that of the downward one. However, in nonlinear magnetization laws, the unstable characteristics of upward and downward waves change close to magnetization saturation. Thus, the general conclusion is that the application force of an arbitrary oblique magnetic field can quantitatively change stability properties. The equation (2.15) represents the non-dimensional magnetic field magnitude relative to the parameter N, which is reciprocal to the pyromagnetic coefficient.

Table 3: The crucial values of parameters Gr, α as well as c for the upward wave of mixed convection under the oblique ($\delta \neq 0^{\circ}$) magnetic field with strength $H^e = 100$ (the lines of odd number), $H^e = 10$ (the lines of even number) for $Gr_m = 12$, $Pr = 27.5$, $\gamma = 0^{\circ}$ with different values for χ and χ_*.

		$\delta = 5^{\circ}$			$\delta = 10^{\circ}$			$\delta = 15^{\circ}$		
χ	χ_*	α_c	Gr_c	c_c	α_c	Gr_c	c_c	α_c	Gr_c	c_c
5	5	0.989	104.50	6.539	0.976	107.38	6.734	0.964	109.64	6.885
		0.993	103.98	6.506	0.979	106.90	6.704	0.966	109.38	6.868
3	5	0.990	104.93	6.575	0.975	108.08	6.790	0.963	110.23	6.932
		0.992	105.05	6.578	0.973	108.23	6.801	0.962	110.24	6.933
3	3	0.991	103.61	6.476	0.986	105.12	6.583	0.976	107.12	6.718
		0.993	103.34	6.459	0.986	105.12	6.583	0.978	106.81	6.697
1.5	2.5	0.994	103.27	6.453	0.987	104.91	6.573	0.978	106.87	6.706
		0.995	103.07	6.441	0.990	104.69	6.555	0.980	106.87	6.702
1	2	0.994	103.24	6.450	0.990	104.37	6.538	0.983	106.04	6.653
		0.995	103.12	6.442	0.993	104.27	6.527	0.981	106.18	6.662
0.5	1.5	0.992	103.80	6.485	0.993	104.09	6.524	0.989	105.13	6.600
		0.993	103.77	6.483	0.992	104.06	6.524	0.989	105.09	6.598

Table 4: The similar values as Table 3 except for the downward wave.

χ	χ_*	$\delta=5^o$			$\Delta=10^o$			$\delta=15^o$		
		α_c	Gr_c	c_c	α_c	Gr_c	c_c	α_c	Gr_c	c_c
5	5	0.987	104.64	-6.548	0.975	107.49	-6.742	0.963	109.70	-6.889
		0.981	105.42	-6.597	0.970	108.04	-6.777	0.963	109.70	-6.889
3	5	0.989	105.44	-6.603	0.971	109.04	-6.845	0.959	111.14	-6.984
		0.985	105.39	-6.606	0.973	108.87	-6.834	0.960	111.12	-6.982
3	3	0.990	103.68	-6.481	0.985	105.22	-6.589	0.975	107.20	-6.723
		0.988	104.04	-6.504	0.981	105.69	-6.619	0.973	107.55	-6.745
1.5	2.5	0.992	103.48	-6.469	0.988	104.95	-6.572	0.978	107.04	-6.714
		0.990	103.72	-6.484	0.985	105.22	-6.592	0.976	107.06	-6.718
1	2	0.992	103.59	-6.475	0.991	104.46	-6.539	0.982	106.37	-6.669
		0.990	103.70	-6.483	0.988	104.57	-6.551	0.983	106.25	-6.661
0.5	1.5	0.988	104.52	-6.536	0.994	104.39	-6.535	0.987	106.05	-6.649
		0.988	104.45	-6.533	0.995	104.35	-6.532	0.987	106.05	-6.649

The pyromagnetic coefficient measures the degree of sensitivity of liquid magnetization to changes in temperature. A higher dimensionless magnetic field corresponds to weaker temperature-dependent liquid magnetization, while a lower non-dimensional magnetic field corresponds to stronger temperature-dependent liquid magnetization. It concludes that, the intensity of the outer magnetic field is directly linked to fluids that exhibit lower and higher thermomagnetic sensitivity. The analysis of Tables 3 and 4 reveals that the implementation of an inclined magnetic field leads to distinct characteristics. In a more thermomagnetically sensitive liquid, the upward propagation wave exhibits a higher number of waves, indicating reduced stability of the basic flow compared to a less thermomagnetically sensitive liquid. These findings hold true irrespective of the linearity of fluid magnetization. It is also observed that whatever the law of fluid magnetization, the upper spreading wave in less thermomagnetically sensitive fluids is faster than in more thermomagnetically sensitive fluids. In contrast, in the context of the upward propagation wave in a more thermomagnetically sensitive liquid, the number of waves is smaller than that of a less thermomagnetically sensitive liquid in an oblique field with arbitrary angles, regardless with the linearity of fluid magnetization. The basic flow of thermomagnetically sensitive liquids appears more stable in relation to downward propagation waves, and the speed of spreading waves increase faster than that of less thermomagnetically sensitive liquids.

The graphs in Figs. 6, 7 and 8 demonstrate the characterizations of the key parameters such as Gr, α as well as c as function of the angle δ of magnetic field with strength of $H^e = 100$, Pr = 27.5, $Gr_m = 12$, but various values of magnetic susceptibilities. In all figures, the plot (a) represents the behavior of Gr (about the flow stability indicates the region below the curves), (b) represents the wave number α, as well as (c) represents the wave speed c, as function of γ in between 0° to 180°. In Fig. 6 (a), the stability results of a given value $Gr_m = 12$ are calculated to analyze the impact of γ denoted as an orientation of magnetic field. Irrespective of the field orientation angle γ, the stability of the basic flow increases with an increment in the field inclination angle δ. When the amount of angle δ

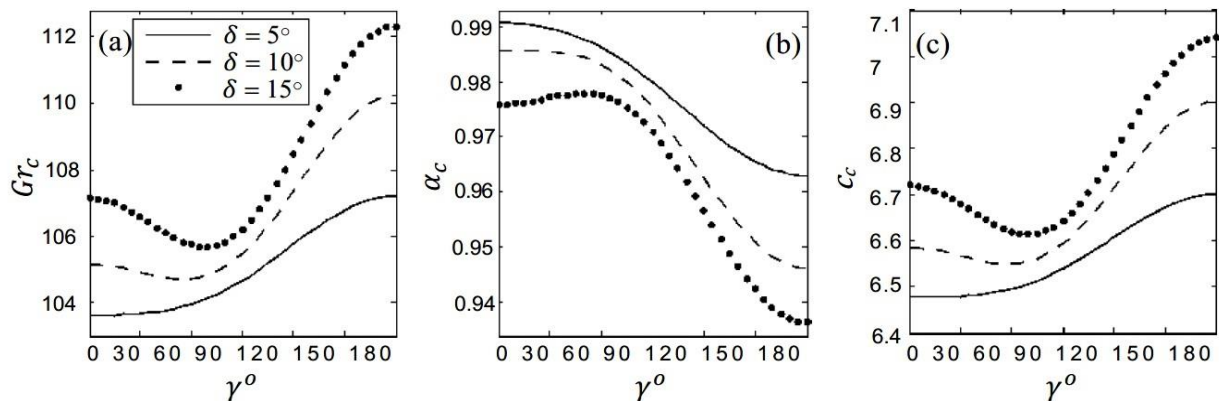**Figure 6:** Comparisons of the crucial values of parameters Gr, α, and c for Pr = 27.5, Gr_m =12, H^e = 100, $\chi = \chi_* = 3$ and $0 \le \delta \le 180°$ with different values of the field angle δ.
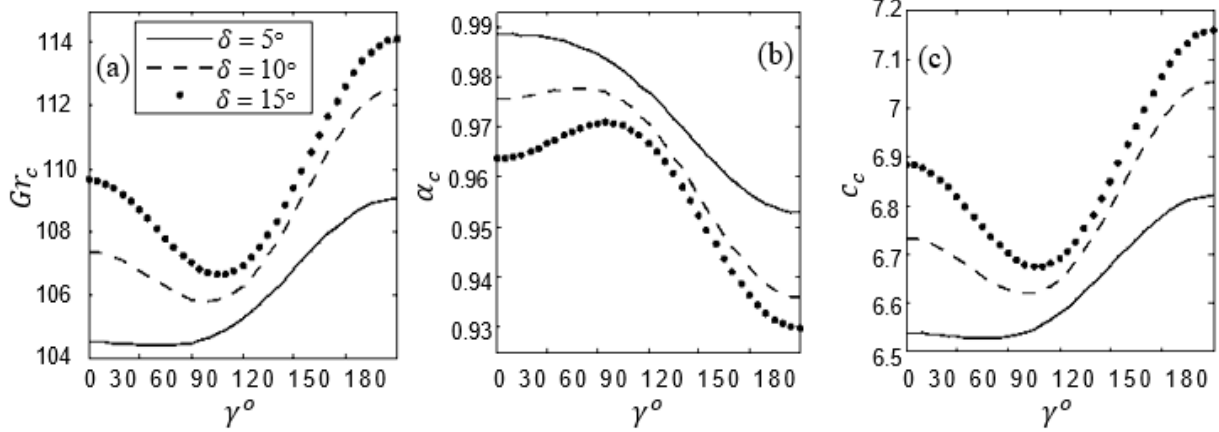
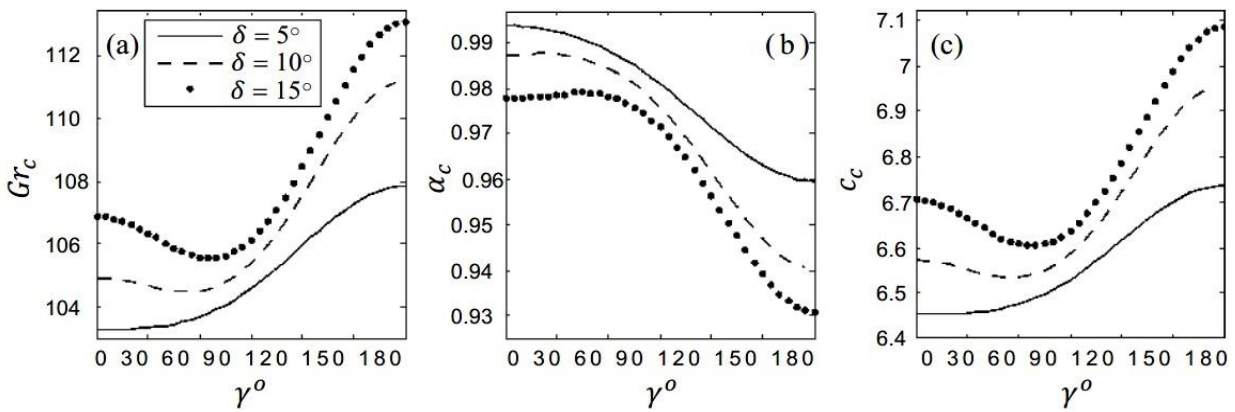**Figure 7:** The similar values as Fig. 6 except for $\chi = \chi_* = 5$

Figure 8: The similar values as Fig. 6 except for $\chi = 1.5$ and $\chi_* = 2.5$.

rises, the wave number reduces with an increase of δ and the distance among the instability rolls rises. The plot (c) in Fig. 6 shows that when the inclination angle of field rises, the speed of the wave increases. The Fig. 7 shows the results of numerical calculations for a more powerfully magnetizable fluid for the value $\chi = \chi_* = 5$. It is observed that, in general, the basic flow of strong magnetizing liquids is more stable than that of weak magnetizing fluids in inclining magnetic fields at any angle. In the existence of linear magnetization law, that is, when $\chi = \chi_*$ the number of waves decreases with the increase in the strength of the magnetic field, and the speed of the wave propagates faster. The Fig. 8 presents the critical values of parameters for nonlinear magnetization laws (for $\chi \neq \chi_*$) closer to magnetic saturation. Comparisons with Figs. 6 and 7 do not allow general comments on flow stability, rather do suggest that the parameters characterizing the stabilization, are dependent on a specific arrangement of values of γ, δ, χ as well as χ_*. Upon comparing the three figures, namely Figs. 6, 7, and 8, it is evident that the basic flow stabilization is predominantly pronounced by the χ, rather than the χ_*. It concludes that, the basic flow of stronger magnetic fluids remains more stable, and its instability pattern is characterized by a smaller number of waves and faster wave speeds than that of weaker magnetic fluids with all magnetic field inclination and orientation angles.

The Figs. 9 and 10, represent the numerical results of Gr, α and c for two prominent waves based on the orientation angle γ ranging between 0 to 180° at Pr = 27.5, He = 100 and $\delta = 5°$ for different values of χ and χ_*. When the magnetic law of the liquid is linear, the parameter curves for both waves exhibit a similar shape, irrespective of the magnitude of fluid magnetization. The findings for $\chi = 3$ and $\chi = 5$ are shown in Figs. 9, and 10 respectively. In the case of the two waves, the difference between any two critical parameters values is likely to be the same in quantity $\gamma > 90°$, that is, when the lines representing the magnetic field pass through the liquid layer from the warm wall to the cold wall upwards. For such field directions, the wave length of the upward spreading wave is slightly shorter in relation to the downward spreading wave. The basic flow of the two waves for $\gamma > 90°$ is unstable with the same values of other parameters. The most noticeable difference quantitatively between $\chi = 3$ and $\chi = 5$ outcomes for the minimal orientation angle γ_{min} of magnetic field. In the case of weak magnetized liquids, the orientation angle for $\chi = 3$ is almost $0°$, while for $\chi = 5$ the orientation angle is almost

43°. The strength of the magnetic effect increases as the maximum field azimuthal angle reaches close to 90°. In nonlinear fluid magnetization laws, the main qualitative observations are that the two waves can be clearly distinguished regardless with orientation angle of the applied field. As a result, in regimes close to the fluid magnetic saturation, the degree of symmetry breaking effect between upward and downward propagation increases.
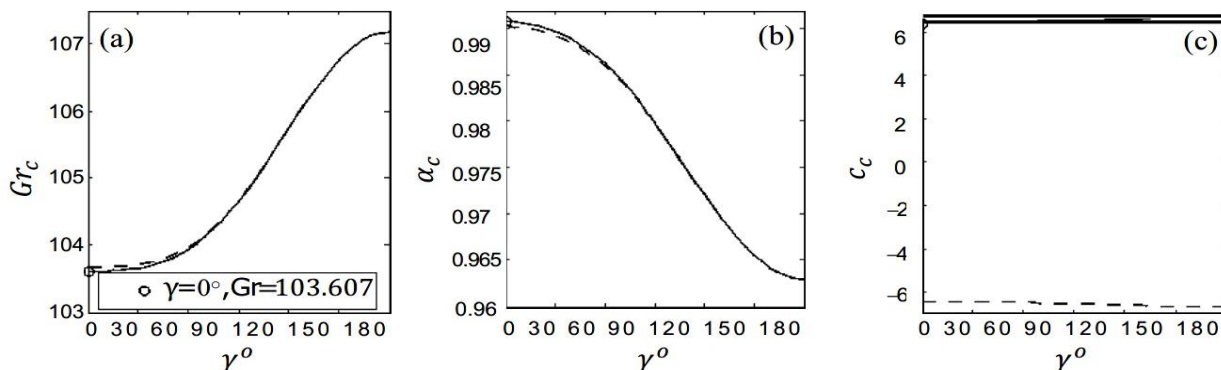

Figure 9: Comparisons of the crucial values of parameters Gr, α, and c as a function of γ for Pr = 27.5, Gr_m = 12, H^e = 100, $\chi = \chi_* = 3$ and $\delta = 5^{\circ}$ for the upward (the solid line) and the downward (the dashed line)
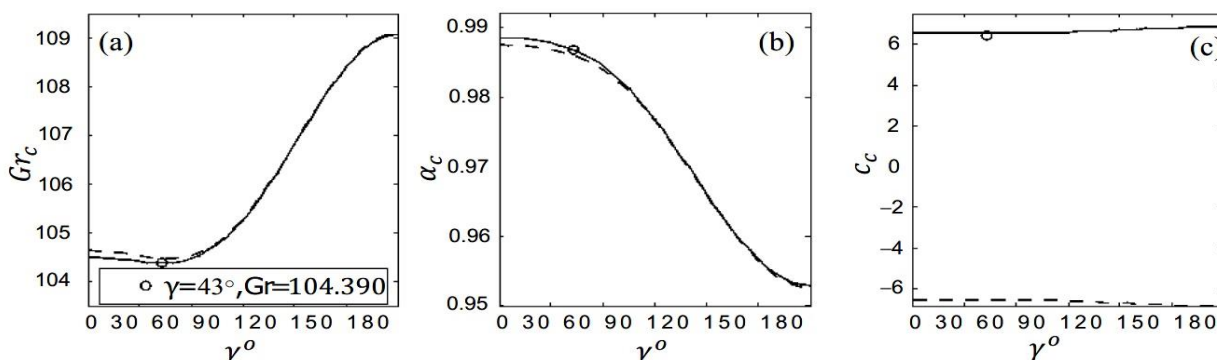
Figure 10: The similar values as Fig. 9 except for $\chi = \chi_* = 5$.

The Figs. 11, 12 as well as 13 examine the stability properties of basic flow and wave-like interruptions are compared for thermomagnetically weaker (for H^e = 100) and more (for H^e = 10) sensitive liquids. The numerical results only for the upward propagation wave are reported in these figures. The thermomagnetically weaker sensitive liquids are more stable related to the highly sensitive liquids.
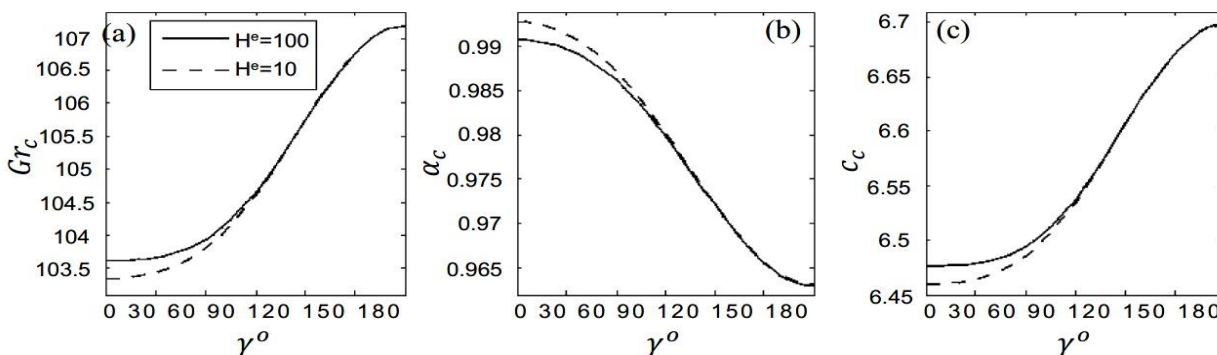

Figure 11: Comparisons of the crucial values of parameters Gr, α, and c as a function of γ for Pr = 27.5, $\chi = \chi_* = 3$, Gr_m = 12 and $\delta = 5^{\circ}$ for thermomagnetically less (H^e = 100) and more (H^e = 10,) responsive fluids.
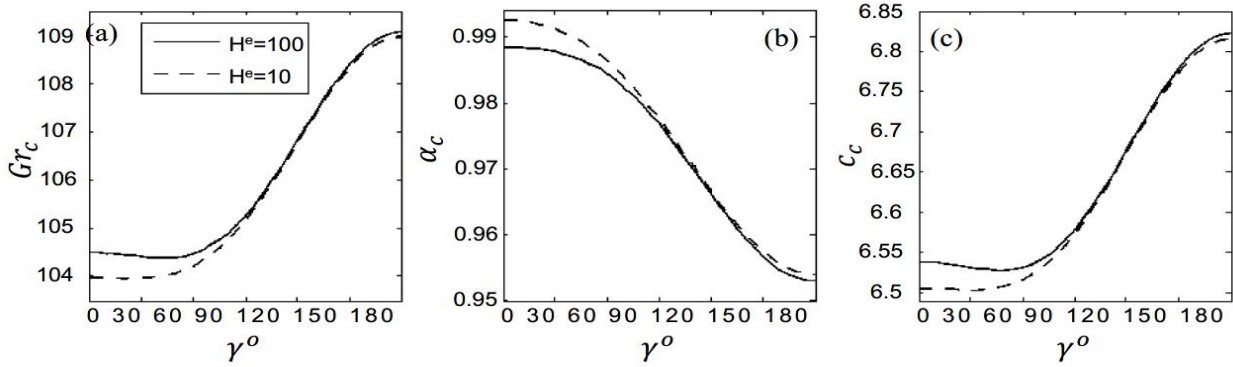
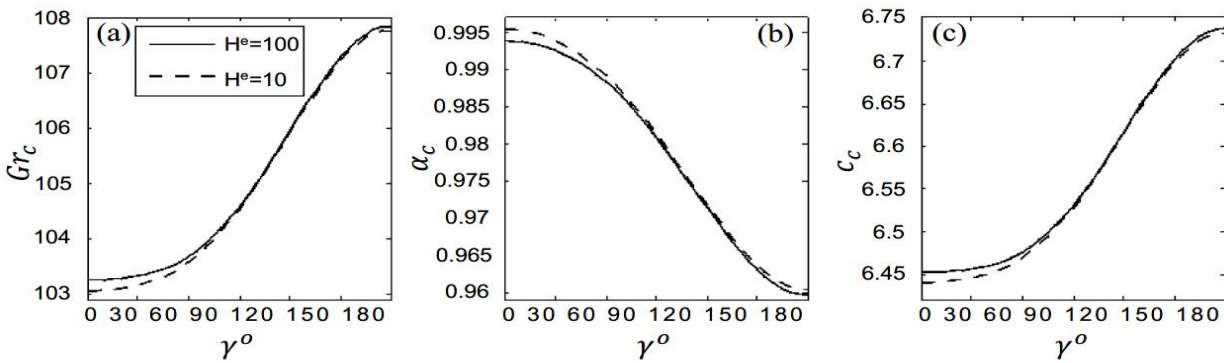**Figure 12:** The similar values as Fig. 11 except for $\chi = \chi_* = 5$.

Figure 13: The similar values as Fig. 11 except for $\chi = 1.5$ and $\chi_* = 2.5$

The difference in critical values of magnetic Grashof numbers, wave numbers as well as wave speed is pronounced highly to the field azimuthal angles ranging from $0°$ to $90°$ irrespective of linear or nonlinear magnetization laws. Furthermore, it is observed that wave-like instability patterns emerge particularly in fluids that are more thermomagnetically sensitive, are characterized by larger wave numbers, and consequently, the convection structures packed more densely in the gravity direction. In addition, the instability waves that occur in less thermomagnetically sensitive fluids have a slightly faster wave speed.

5. STABILITY DIAGRAMS OF FLUID FLOWS

In this section, we identify and discuss the parametric regions in which different physical mechanisms produce instability thresholds in the geometry of the present problem. The stability diagrams corresponding two-dimensional pattern are investigated here to characterize the physical phenomena. The flow instability resulting from different critical values of Gr and Gr_m, as well as the corresponding number of waves and wave speeds are shown in Fig. 14 for the particular values of $\gamma = 0°$, $H^e = 100$, $\chi = \chi_* = 5$, and Pr = 27.5 are accounted for the normal field. It is seen that; this stability diagram is divided into three branches that depict the three types of instabilities. The solid line in the figure (a) of Fig. 14 relates to the instability mode of the thermogravitational convection, which begins at $Gr_m = 0$ and Gr = 108 (approximate) and characterizes the stability more than that depicted in Fig. 15 reported in (Rahman & Suslov, 2016) as there used Pr = 55.

The associated wave numbers are shown in diagram (b) and the wave velocity in diagram (c), in the Fig. 14. The plot (c) clearly shows that there exist two waves that propagate in the opposite directions. The dashed line represents the magnetic convection instability mode, which begins at Gr = 0. The instability begins at Gr ≠ 0, Gr_m ≠ 0, which is defined as magneto gravitational convection, as seen by the dashed dotted line in the Fig. 14. It is obvious that thermogravitational convection instability develops in low waves; magnetic convective instability happens at intermediate waves as well as magneto gravitational convection instability develops in higher waves. The numerical results displayed in Fig. 14 are qualitatively comparable to those results displayed in Fig. 15 analyzed in (Rahman & Suslov, 2016), but quantitatively different due to various Pr values estimated here. The plot (a) in Fig. 14 indicates that fluid convection flow is stable over the dashed as well as dash-dotted lines and underneath the solid line. The graphs in Figs. 16 and 17 displayed with the same parameter values as Fig. 14 but with different values of field inclination angle δ. The Figs. 16 and 17 demonstrate the stability diagrams in a similar fashion under magnetic effects with different inclination angles $\delta = 5°$ and $\delta = 10°$ respectively. However,

there are qualitative similarities to the Fig. 12 (for $\delta = 5^\circ$), which reported in (Rahman & Suslov, 2016), but numerically it vary. It is obvious from the plots in Figs. 14, 16, 17 that the inclination angles of magnetic field bear a major impact in the flow domain's instability features.
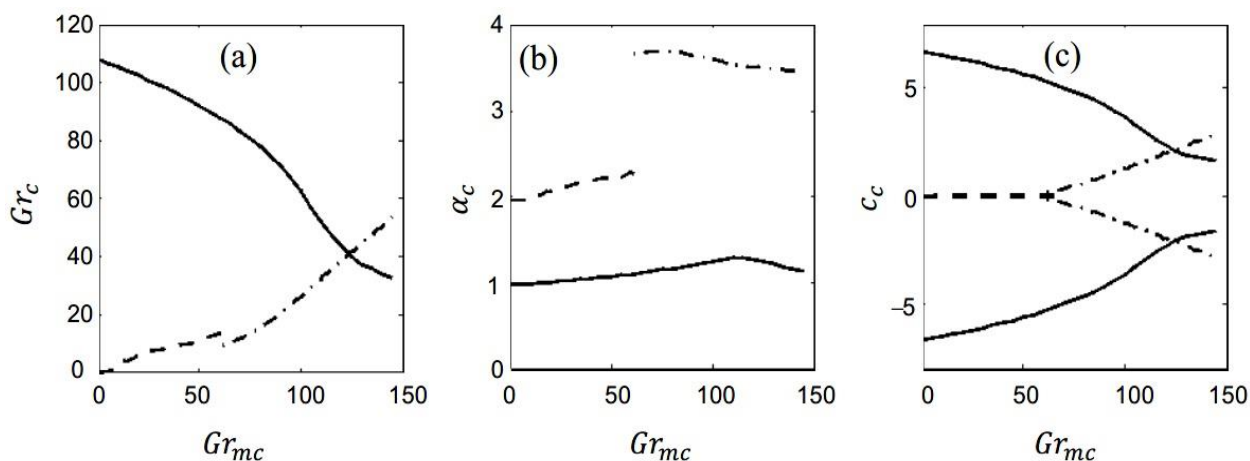

Figure 14: (a) The stability figure related to two-dimensional pattern; (b) the crucial wave number α as well as (c) the spreading wave speed for $H^e = 100$, $\chi = \chi_* = 5$, Pr = 27.5, and $\delta = 0^\circ$.
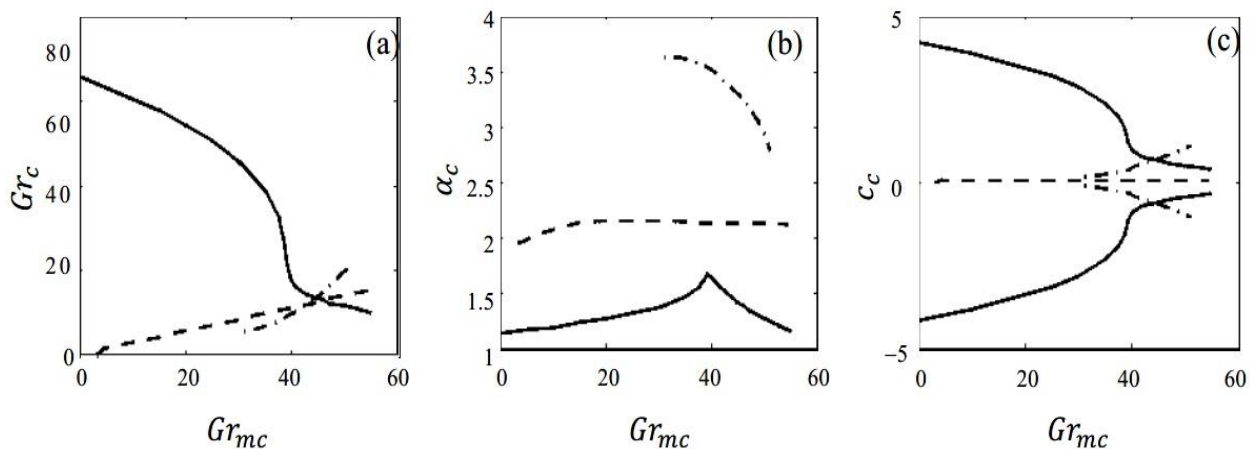

Figure 15: (a) The stability figure related to two-dimensional pattern; (b) the crucial wave number α as well as (c) the spreading wave speed for $H^e = 100$, $\chi = \chi_* = 5$, Pr = 27.5, and $\delta = 0^\circ$ as depicted Fig. 12, reported in (Rahman & Suslov, 2016)
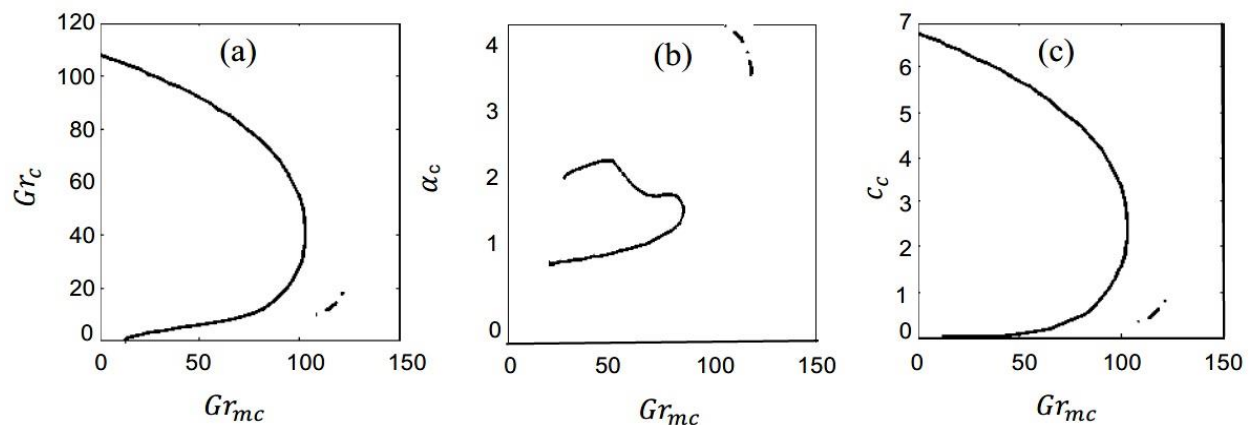

Figure 16: (a) The stability figure related to two-dimensional pattern; (b) the crucial wave number α as well as (c) the spreading wave speed for $H^e = 100$, $\chi = \chi_* = 5$, Pr = 27.5, $\gamma = 0^\circ$ and $\delta = 5^\circ$ (oblique magnetic field).
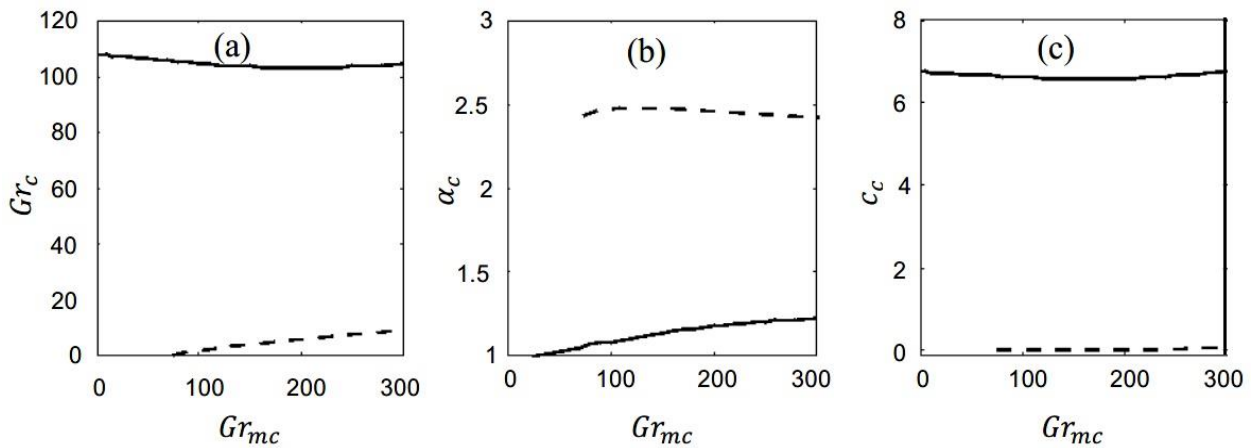
Figure 17: (a) The stability figure related to two-dimensional pattern; (b) the crucial wave number α as well as (c) the spreading wave speed for $H^e = 100$, $\chi = \chi_* = 5$, $Pr = 27.5$, $\gamma = 0°$ and $\delta = 10°$ (oblique magnetic field).

The solid and dashed stability boundary lines are distinguishable as seen from Fig. 14 (a) but they merged in 16, indicating that the difference between thermal and magnetic instabilities is blurred when the magnetic field is inclined at $\delta = 5°$. An ambiguity arises for $\delta = 10°$ and the magneto gravitational instability can hardly be detected. The solid and dashed lines become entirely separated as the field inclination angle increases. The attribute corresponds to the observation made by Rahman and Suslov (2016). It is seen that any alteration in an amount of the Prandtl number having an effect on flow stabilization, and it can therefore be inferred that a change in quantity in the stability diagram happens for various amounts of the Prandtl number of fluids. Overall, it is clear from the explanation of this paper, the basic flow remains stable comparatively more and wave propagation is faster in smaller values of Pr comparing to the greater values of Pr as the discussion in (Rahman & Suslov, 2016). However, the spreading wave has smaller number of waves in fluids with a smaller Prandtl number than those with greater Prandtl number of fluids.

6. CONCLUSIONS

For analysis and comparison, we considered a different type of fluid other than that investigated in (Rahman & Suslov, 2016). The stability properties of the basic flow of the thermomagnetically weaker sensitive fluids and more sensitive fluids are analyzed. For a variety of magnetic susceptibilities, the critical values of important controlling parameters for both linear and nonlinear magnetizable fluids for the problem are computed and analyzed. According to the obtained results and discussion, a number of conclusions can be drawn as:

- The thermal and magnetic effects in fluids for variant Prandtl number are in agreement with previous studies on pure gravitational convection.
- The wave speed has no dependency on Prandtl number at the threshold of static magneto convection.
- In each thermomagnetically high and low sensitive fluids in the entire area of the flow domain, the upward spreading wave continuing to be the more hazardous as compared to that of the downward wave.
- In general, the stability properties can alter qualitatively as the applied magnetic field strength and its directional angle increases.
- A comparison of the subsequent stability figures with those described in (Rahman and Suslov, 2016) demonstrates that under both the normal and oblique magnetic fields, smaller Prandtl number of fluids exhibit more stable basic flows and faster wave propagation than larger Prandtl number of fluids.

In this article, the main assumption is that the considered fluid has a homogeneous composition. In reality this may not always be the case due to gravitational sedimentation, thermo- and magneto-diffusion effects. Thus, extending this study to incorporate thermo-diffusion effect for the future study might be a logical recommendation. Another non-trivial extension of this study could be to take into account the flow stability in a layer inclined with the gravitational direction and placed in a magnetic field with arbitrary orientation.

NOMENCLATURE

η_*	Dynamic viscosity	t	Time
f	Volume concentration of magnetic phase	T	Temperature
ρ_*	Density	p	Pressure
β_*	Coefficient of thermal expansion	B	Magnetic flux density
k_*	Thermal diffusivity	Gr	Thermal Grashof number
K	Pyromagnetic coefficient	$\mathrm{Gr_m}$	Magnetic Grashof number
μ_*	Magnetic constant	Pr	Prandtl number
H^e	External magnetic field	N	Strength of the magnetic field
T_*	Average (reference) temperature in the layer	α	Wave number
2Θ	Temperature difference between the walls	c	Wave speed
$2d$	Distance between the walls	δ	Magnetic field inclination angle
χ	Magnetic susceptibility	γ	Magnetic field Azimuthal angle

REFERENCES

Albrecht T., Bhrer C., Fhnle M., Maier K., Platzek D., & Reske J., (1997). First observation of ferromagnetism and ferromagnetic domains in a liquid metal, Appl. Phys. A-Mater., 65(2), 215–220.

Belyaev A. V., and Smorodin B. L., (2010). The stability of ferrofluid flow in a vertical layer subject to lateral heating and horizontal magnetic field, J. Magn. Magn. Mater., 322, 2596–2606.

Bozhko A. A., & Putin G. F., (1991). Experimental investigation of thermo-magnetic convection in uniform external field, Bulletin of the Academy of Sciences of the USSR. Physical series, 55, 1149–115.

Bozhko A. A., Pilugina T. V., Putin G. F., Shupenik D. V., & Suhanovsky A. N., (1998). On instability of thermogravitational flow in a ferrofluid vertical layer in the transversal magnetic field, In Yu. Ya. Schelykalov, editor, Proc. of the 8th International Conference on Magnetic Fluids, Plyos, Russia, 75–78.

Bozhko A.A., & Putin G.F., (2003). Heat transfer and flow patterns in ferrofluid convection, Magnetohydrodynamics, 39, 147–169.

Bozhko A.A., Putin G.F., Sidorov A.S., & Suslov S.A., (2013). Convection in a vertical layer of stratified magnetic fluid Magnetohydrodynamics, 49, 143–152.

Chamkha A. J., Rashad A. M., & Alsabery A. I., (2020). Impact of partial slip on magneto-ferrofluids mixed convection flow in enclosure. Journal of Thermal Science and Engineering Applications, 12, 051002.

Finlayson B.A., (1970). Convective instability of ferromagnetic fluids, J. of Fluid Mechanics, 40, 753–767.

Hatziavramidis D., & Ku H. C., (1985). An integral Chebyshev expansion method for boundary-value problems of O.D.E. type, Comput. Math. Appl., 11(6), 581-586.

Ku H. C., & Hatziavramidis D., (1984). Chebyshev expansion methods for the solution of the extended Graetz problem, J. Comput. Phys., 56, 495-512.

Odenbach S., (2002). Ferrofluids: magnetically controllable fluids and their applications, Springer, New York.

Rahman H., & Suslov S. A., (2015). Thermomagnetic convection in a layer of ferrofluid placed in a uniform oblique external magnetic fluid, Journal of Fluid Mechanics, 764, 316–348.

Rahman H., & Suslov S. A., (2016). Magneto-gravitational convection in a vertical layer of ferrofluid in a uniform oblique magnetic fluid, Journal of Fluid Mechanics, 795, 847–875.

Rosensweig R. E., (1985). Ferrohydrodynamics, Cambridge University Press.

Suslov S. A., (2008). Thermo-magnetic convection in a vertical layer of ferromagnetic fluid, Physics of Fluids, 20(8), 084101.

Suslov S.A., Bozhko A.A., Sidorov A.S., & Putin G.F., (2012). Thermomagnetic convective flows in a vertical layer of ferrocolloid: Perturbation energy analysis and experimental study, Phys. Rev. E, 86, 016301.

Taskesen E., Dirik M., Tekir M., & Pazarlioglu H. K., (2023). Predicting heat transfer performance of Fe3O4-Cu/water hybrid nanofluid under constant magnetic field using ANN. Journal of Thermal Engineering, 9, 811-822.